

The Potential for Incorrect Interpretation of Atmospheric Images as Seen with OSIRIS.

D.A. Degenstein, E.J. Llewellyn, and N.D. Lloyd

ISAS, University of Saskatchewan, 116 Science Place, Saskatoon, SK Canada

Received: 6.2.2002 – Accepted: 14.10.2002

Abstract. The Odin satellite that was launched on February 20, 2001, includes an Optical Spectrograph and Infra-Red Imaging System (OSIRIS). During each orbit OSIRIS makes many thousand line integral measurements of the atmospheric volume emission rate profiles at wavelengths of 1.27 μm and 1.53 μm that are ideal for interpretation with a tomographic technique. The adopted tomographic technique uses the line of sight integrated volume emission measurements and a modified Maximum Likelihood Expectation Maximization (MLEM) algorithm to retrieve two dimensional structure in the atmospheric volume emission profile. The utility of the developed tomographic technique is demonstrated with examples from the OSIRIS data set. It is shown that the correct interpretation of the two-dimensional volume emission rate profiles can be obtained with the use of limb imaged data and the tomographic analysis. It is also shown that the simple one dimensional analysis of single limb scans may lead to significant errors in the apparent structure of the volume emission profiles. The capability of the OSIRIS measurements for the determination of small and large-scale horizontal structures in the Oxygen Infra-Red Atmospheric and the OH Meinel band emissions is demonstrated with some of the first on-orbit observations made with the OSIRIS Imager.

1 Introduction

OSIRIS, the Optical Spectrograph and InfraRed Imaging System on the Swedish satellite Odin is comprised of an Optical Spectrograph (OS), that measures scattered sunlight over a wavelength range from 280 to 800 nm, and an InfraRed Imager (IRI), that measures both scattered sunlight and airglow emissions within three distinct passbands. Channel One is designed to measure nighttime OH and daytime scattered sunlight while, for redundancy, both Channels Two and Three measure the Oxygen InfraRed Atmospheric band (OIRA) spec-

trum in slightly different wavelength ranges. Each channel of the IRI consists of a single lens and a linear InGaAs detector array that has 128 pixels. The limb brightness is imaged on to 100 of these pixels while 28 pixels are masked off to provide dark current and DC offset calibration information. The 100 pixels that are illuminated cover approximately a 2 field of view with almost 1 km tangent altitude resolution in the vertical. The Odin orbit is essentially circular at an altitude of 600 km and an inclination of 97.

2 The Data

During May 2001, there was a commissioning phase for the OSIRIS instrument. At that time the optical axes of the IRI channels, all three are approximately co-aligned, were made to stare at a tangent altitude of 53 km and a series of 5191 images, shown as a collage in Figure 1, were collected for each of the three channels. During the six hours of data collection the satellite completed almost four orbits. The daytime and nighttime parts of the orbits are clearly distinguishable in Figure 1. During the nighttime part of the orbit only a small high altitude signal, centred near pixel 50, is visible in Channel One. This is the OH Meinel band airglow emission. This signal is quite different from that seen during the daytime where Rayleigh scattered sunlight is dominant and the signal appears to increase exponentially with decreasing pixel number (tangent altitude). The apparent high altitude daytime signal is an instrumental effect. This scattered light is believed to be a diffraction limit effect that must be removed in the full analysis. At this time an effective scattered light removal technique has been completed but it is not yet fully implemented.

It is readily apparent from Figure 1 that Channels Two and Three produce nearly identical data sets; this is expected from the filter passband positions. The day and night portions are easily identifiable in these two data sets as the OIRA band is primarily formed through ozone photolysis and so is much brighter during the daytime. The nighttime signal is

Correspondence to: D.A. Degenstein

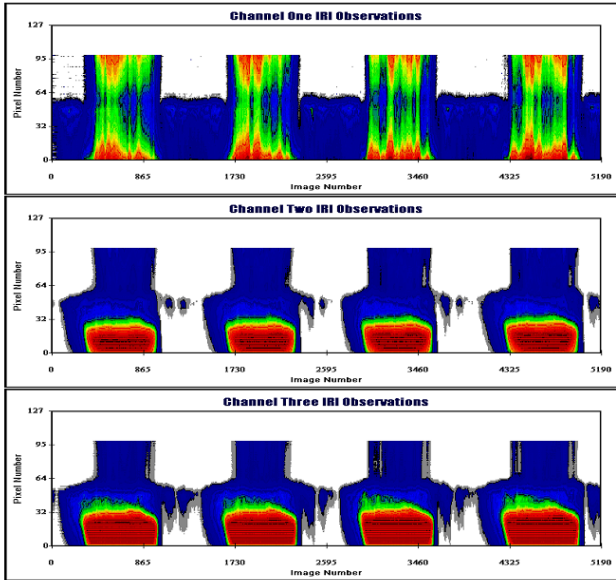


Fig. 1. Three IRI data sets, one for each channel, collected during the commissioning. The optical axes of each channel stared at approximately 53 km.

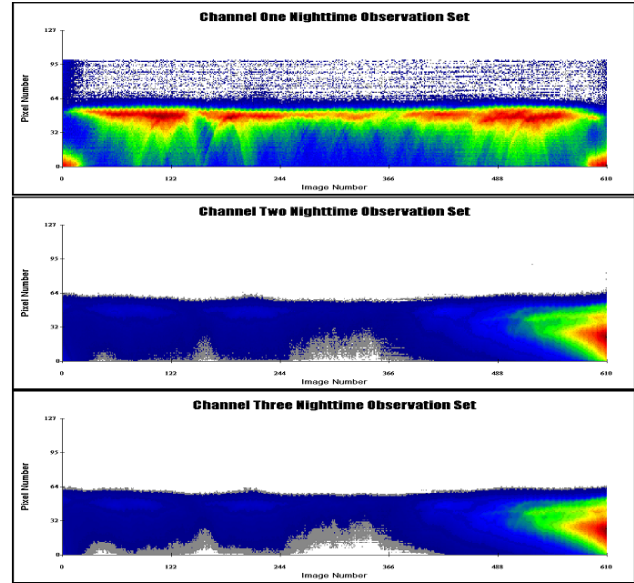


Fig. 2. The nighttime portions of the first orbits seen in Figure 1. Channel One shows the nighttime OH while Channels Two and Three illustrate the nighttime OIRA band.

at high altitude, also near pixel 50, and is what remains after the daytime excited emission has decayed. As with the OH emission channel both channels two and three are affected by the high altitude scattered light during the daytime observation period. The data produced by the IRI channels has not yet been absolutely calibrated so that intensity units are omitted from the shown figures. As already noted the data sets shown in Figure 1 include both daytime and nighttime measurements. The measurements shown in Figure 2 are a subset of those in Figure 1 and are the first nighttime data set, centred around image 1200. These nighttime measurements include data from all three channels and it is of interest to note, in the first plot of Figure 2, the regions of enhancement in the nighttime OH limb profile both just before sunrise (the left side) and just after sunset (the right side). The enhancements in the lowest pixels at each end of the plot are due to the scattering of sunlight in the lower atmosphere. This figure also shows the two measurement sets of the twilight and nighttime OIRA band emissions. Here the dusk side decay in the limb profile is very evident and appears to contain significant small-scale structure.

The data sets shown in Figure 1 also contain another very interesting feature that is barely visible in these complete data sets. In the second complete nighttime portion of the Channel One data set there appears to be an enhancement on the dawn (left) side. Figure 3 is an expansion of this nighttime data and clearly indicates the enhancement in the limb brightness profile. The inverted U structure in the observation set is typical of a localized increase in volume emission rate. The image-numbering scheme has been changed in this figure and the colour scale of the plot modified in order to add greater contrast to the enhancement. The single image cross-sections, that represent the vertical limb brightness profile,

reveal a number of interesting features for the enhancement shown in the upper plot of Figure 3. The four limb profile plots shown in Figure 3 contain 17 single image cross sections from the entire data set. These cross sections are taken at equal time (or distance) intervals along the orbit track and illustrate the effects of a localized enhancement in the two-dimensional (vertical and horizontal) volume emission profile on the one-dimensional limb image. It is clear that the limb intensity profiles contain bifurcations that would appear to indicate a bifurcated vertical volume emission rate profile.

3 The Inversion Technique

Tomography is the representation of a three-dimensional object by its two-dimensional cross sections and the tomographic concept uses line integral measurements of a two-dimensional field to retrieve that field. The tomographic technique that is used in the present work, to retrieve the two-dimensional volume emission rate airglow profile from the OSIRIS Infra-Red Imager measurements, is based on the Maximum Probability technique proposed by Lloyd and Llewellyn (1989) to de-blur Fabry-Perot images. McDade et al. (1991a, 1991b, 1993) showed that this technique could also provide meaningful retrievals from atmospheric brightness measurements. In the current modified Maximum Likelihood Expectation Maximization technique (Degenstein, 1999) the developed algorithm assumes a discrete volume emission grid with boundaries that delimit shell altitudes and angles along the satellite track. This grid and the geometry for a discrete measurement are shown in Figure 4. The equations beneath Figure 4 are the modeled representation of the brightness that would be measured along the line of sight shown in this figure. In these

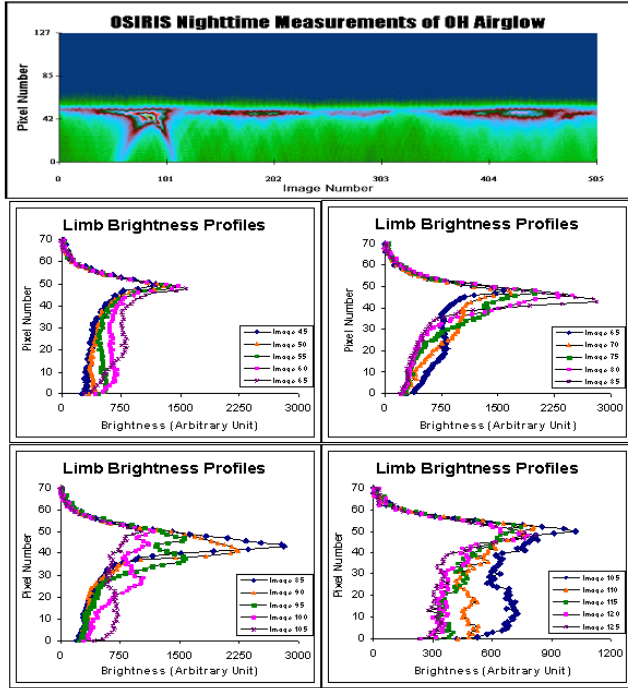
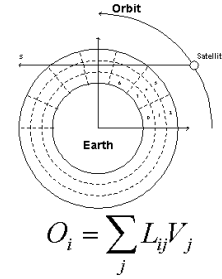


Fig. 3. The nighttime portion of the second Channel One orbit seen in Figure 1. The inverted U feature in the two-dimensional limb brightness profile is typical of a localized enhancement in the volume emission rate profile. Also included in this figure are a series of evenly spaced image cross sections that clearly indicate a bifurcated limb brightness profile.

equations O_i is the observed brightness, V_j is the volume emission rate associated with cell j and L_{ij} is the geometric path length of the i^{th} observation through the j^{th} cell. The tomographic equations and a block diagram of the retrieval technique (Degenstein, 1999) are illustrated in Figure 5. It is apparent that the recovery algorithm is an iterative Multiplicative Algebraic Reconstruction Technique (MART) that uses only the measurements and the geometry to determine the initial solution and each iterative result. The termination criterion for the iteration process is a set number (usually 30) of iterations. If the inversion parameters, such as the grid cell size and the observation weighting parameter b , are correctly chosen then the solution always converges and no upper limit to the iteration number is required.

4 Modeled Enhancement

The apparent bifurcation in the limb emission profiles shown in Figure 3 was studied through an investigation of the effects of localized enhancements on both the observations and the retrievals. The two-dimensional volume emission rate profile and the associated observations are shown in Figure 6. The volume emission rate profile that is presented in the first plot of this figure has a localized enhancement superimposed upon a typical background emission. The simulated observation set contains the same inverted U structure that is seen in Figure 3 and the limb brightness profiles, or image cross-



$$O_0 = L_{0,8}V_8 + L_{0,7}V_7 + L_{0,10}V_{10} + L_{0,13}V_{13} + L_{0,14}V_{14}$$

Fig. 4. The geometry of the tomographic retrieval grid. This figure also includes the simple model representation of the brightness measured along the line of sight s.

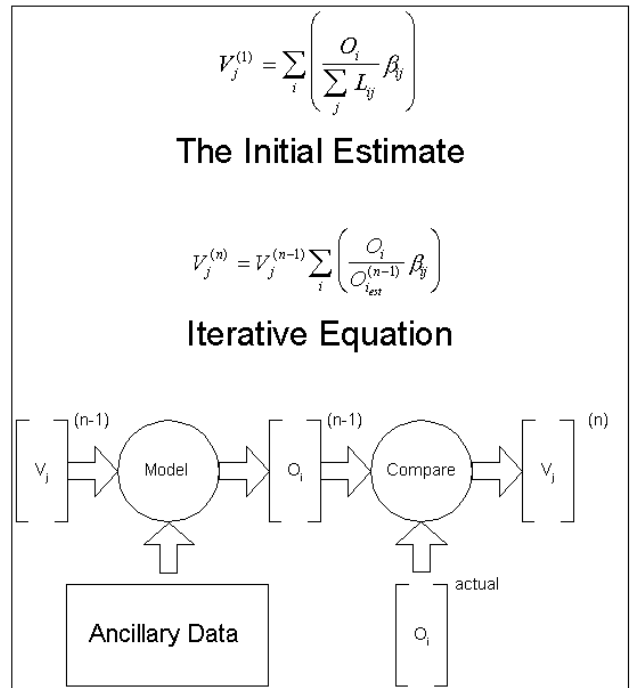


Fig. 5. The tomographic equations and the block diagram of the retrieval technique.

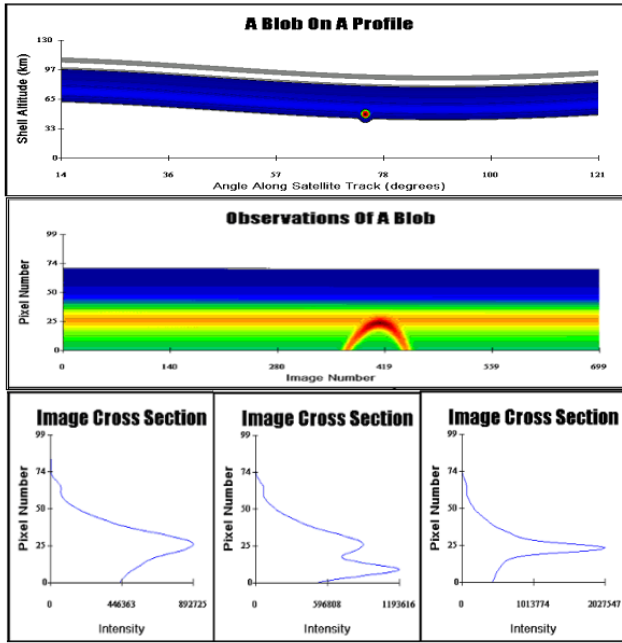


Fig. 6. A modeled enhancement superimposed on a typical vertical volume emission rate profile. The grid in this plot is an earth centred radial grid. This figure includes a set of observations of the modeled profile along with three sample limb images. Note the bifurcation.

sections, contain bifurcations that are not present in the volume emission profile. The retrieval of the data presented in Figure 6 is shown in Figure 7. The tomographic routine has recovered the localized enhancement and without adding a bifurcation to the vertical profile. The bifurcation would necessarily have been present in any one-dimensional retrieval scheme. For this figure the two-dimensional volume emission rate profiles have been plotted on an altitude-angle grid instead of the radial grid used in Figure 6.

5 The Retrieval Results

The results of the first tomographic retrievals that were done with the IRI data are shown in Figure 8. These retrievals used the nighttime data shown in Figure 2. It is apparent that the OH nightglow profile is enhanced in both the dawn (left) and dusk (right) and is eroded from below in the evening twilight. It is also apparent that there is an abundance of small-scale features in the OIRA band emissions at dusk, just after the daytime emission has lost its primary excitation source. These plots were made at ESRANGE, in Northern Sweden, during commissioning and therefore the attitude information used in the retrievals is coarse. For this reason there may be a systematic error in the altitude profiles of the recovered emission features.

The results of a tomographic retrieval that used the Channel One data shown in Figure 3 are presented in Figure 9. In this case the emission enhancement that is readily visible in the observation data has been correctly retrieved and is clearly seen in the dawn sector of the nighttime part of the

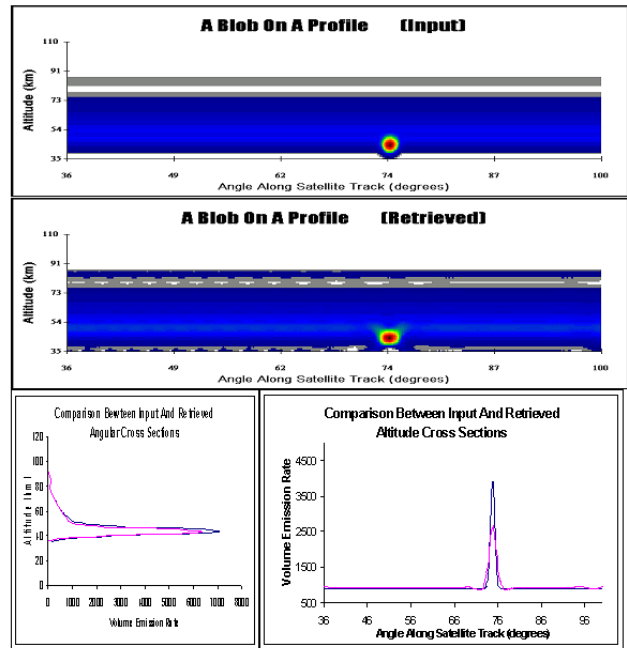


Fig. 7. The retrieval of the input data presented on an altitude and angle grid. Also shown are two cross sections that compare the input with the retrieved values. The retrieval technique recovers and almost fully resolves the small-scale structure.

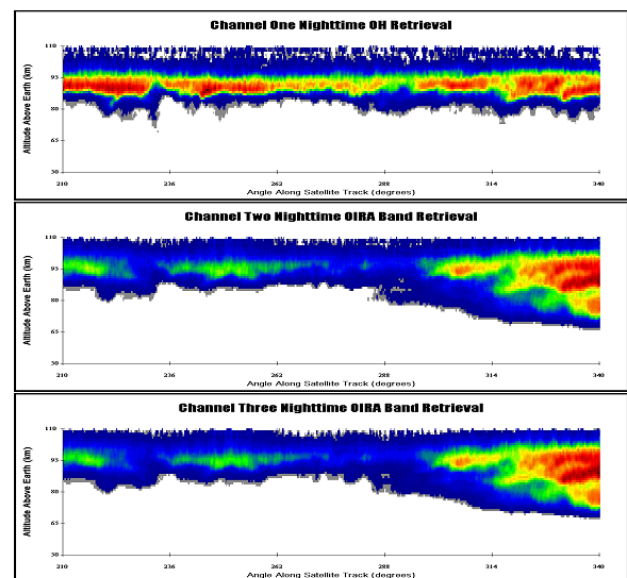


Fig. 8. The first tomographic retrievals for the nighttime data sets that are shown in Figure 2.

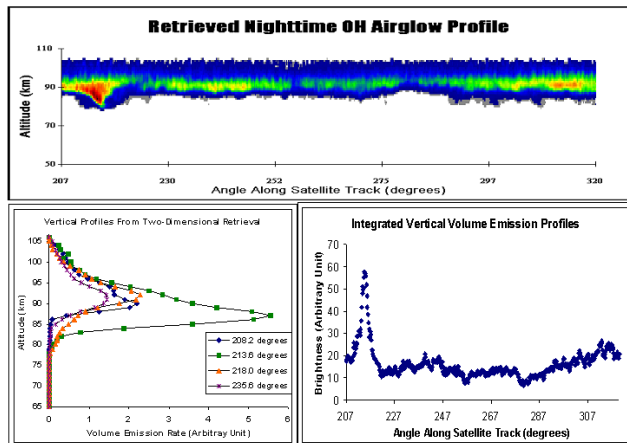


Fig. 9. The retrieval of the enhancement seen in the data set shown in Figure 3. Also included are vertical volume emission rate cross-sections and a total integrated profile.

orbit.

Cross sections of the retrieved results are shown in the second plot in Figure 9. These indicate an enhancement and a lowering in altitude of the peak of the OH emission profile at a retrieval grid angle of 213.6. The peak of the volume emission rate profile is enhanced by about a factor of 4.5 from its normal value at 235.6. However, the observations, Figure 2, indicate only an enhancement of a factor of 3. This is typical of localized enhancements viewed in the limb. The line of sight observations are not enhanced by the same factor as the volume emission rate profile. The integrated overhead profile for each angle along the satellite track is also included in this figure. This plot shows that there is a significant increase in the total OH airglow at the same location as the localized enhancement.

6 Conclusions

The OSIRIS IRI, with Odin in the stare mode, produces data that is well suited for input to the modified MLEM tomographic retrieval technique. The two-dimensional recovery algorithm is able to correctly identify small-scale structures where one-dimensional retrieval techniques would fail.

References

- Degenstein, D.A., Atmospheric Tomography. *Ph.D. Thesis*. University of Saskatchewan, Saskatoon, Canada, 1999.
- Lloyd, N.D. and E.J. Llewellyn, Deconvolution of blurred images using photon counting statistics and maximum probability, *Can. J. Phys.*, 67, 89, 1989.
- McDade I.C., N.D. Lloyd and E.J. Llewellyn, A rocket tomography measurement of the 3914 emission rates within an auroral arc, *Planet. Space Sci.*, 39, 895, 1991a.
- McDade, I.C. and E.J. Llewellyn, Inversion techniques for recovering two-dimensional distributions of auroral emission rates from rocket photometer measurements, *Can. J. Phys.*, 69, 1059, 1991b.

McDade, I.C. and E.J. Llewellyn, Satellite airglow limb tomography: methods for recovering structured emission rates in the mesospheric airglow layer, *Can. J. Phys.*, 71, 552, 1993.